Received: 31 March 2024 | Revised: 14 May 2024 | Accepted: 30 May 2024

DOI: 10.1002/ppap.202400078

PLASMA PROCESSES AND POLYMERS

RESEARCH ARTICLE

Study of a full coaxial atmospheric pressure plasma jet device and its application to the modification of polytetrafluoroethylene

Dai Zhang[1] | **Shuchang Xu**[1] | **Zhenguo Hou**[2] | **Xijiang Chang**[1] | **Zhonghang Wu**[3] | **Zilan Xiong**[2]

[1]College of Science, Donghua University, Shanghai, People's Republic of China

[2]State Key Laboratory of Advanced Electromagnetic Technology, Huazhong University of Science and Technology, Wuhan, Hubei, China

[3]Shanghai Key Laboratory of Molecular Imaging, Shanghai University of Medicine and Health Sciences, Shanghai, People's Republic of China

Correspondence

Xijiang Chang, College of Science, Donghua University, Shanghai 201620, People's Republic of China.
Email: changxj@dhu.edu.cn

Zhonghang Wu, Shanghai Key Laboratory of Molecular Imaging, Shanghai University of Medicine and Health Sciences, Shanghai, 201318, People's Republic of China.
Email: wuzh@sumhs.edu.cn

Zilan Xiong, State Key Laboratory of Advanced Electromagnetic Technology, Huazhong University of Science and Technology, Wuhan, Hubei, 430074, People's Republic of China.
Email: zilanxiong@hust.edu.cn

Funding information

National Natural Science Foundation of China, Grant/Award Numbers: 12175035, 12375251, 12005128; Open fund of State Key Laboratory of Advanced Electromagnetic Technology, Grant/Award Number: 2022KF009; the Fundamental Research Funds for the Central Universities, Grant/Award Number: 2232024D-29

Abstract

In this article, a compact and portable microwave atmospheric pressure plasma jet (MW-APPJ) generator based on a coaxial transmission line resonator (CTLR) was proposed. Based on the electromagnetic simulations, the jet generator was designed as a tapered inner conductor structure that ensures plasma generation at low power. A self-igniting argon (Ar) plasma jet of 10 mm length was generated at an input power of ~20 W and maintained at 2 W. Thanks to the high efficiency of the CTLR structure, plasmas of mixed reactive gases were also realized. Intrinsic plasma parameters and active species were determined using optical emission spectroscopy. Furthermore, the MW-APPJ device was used to modify the polytetrafluoroethylene surface, and improvement of hydrophilicity was achieved without thermal damage.

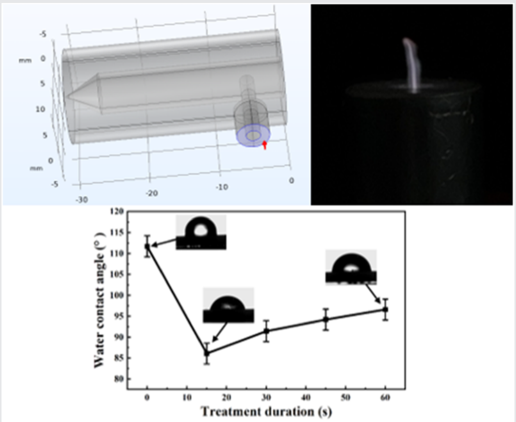

KEYWORDS

atmospheric pressure plasma jet, coaxial transmission line resonator, plasma diagnostics, surface modification

1 | INTRODUCTION

Atmospheric pressure plasma jets (APPJs) are attracting more and more attention due to their ability to generate high-density, low-temperature plasma directly in open space, which makes them easy to use in a variety of applications, such as materials surface modification, thin-film deposition, biomedicine, aerospace, environmental sciences, and so on.[1–5] APPJ can be generated in a variety of approaches, similar to low-pressure plasma, such as direct current, low-frequency alternating current, radio frequency, and microwave. It has been reported that the APPJ device operating at 2.45 GHz offers several advantages compared with those operating at radiofrequency (rf, 13.56 MHz) and kilohertz frequencies.[6] First, the 2.45 GHz frequency range allows for more efficient energy transfer to the plasma, resulting in higher plasma density and a more effective treatment process. The plasma density of MW-APPJ is 1–2 orders of magnitude higher than that of jet devices working on rf and kilohertz frequencies. Higher plasma density offers higher concentration of active species that play a pivotal role in surface modifications of materials. Second, operating at 2.45 GHz provides finer control over the plasma parameters, such as gas temperature, plasma density, and active species, which allows for enhanced treatment performance and versatility. Last, operating at 2.45 GHz typically results in lower levels of electromagnetic interference compared with rf and kilohertz frequencies, which can minimize interference with nearby electronic devices and improve the safety and reliability of the plasma treatment system. In addition, without the need of a vacuum system benefiting from atmospheric pressure discharge, the overall portability of the device can be greatly enhanced. In this way, the microwave atmospheric pressure plasma jet (MW-APPJ) can be more conveniently used in biomedical and material processing applications.

In recent years, research on MW-APPJ has been carried out extensively, and various MW-APPJ device structures and related applications have been proposed. Chen et al.[7] designed a surface-wave plasma jet based on the theory of surface plasmon. The microwave power was coupled from a flat rectangular waveguide to a cylindrical quartz tube through a single-pin antenna and then propagated to the end of the quartz tube through surface waves to generate a discharge, which produced a filamentary streaming plasma jet at low power (minimum 20 W). Choi et al.[8] designed a coaxial transmission line resonator (CTLR) type MW-APPJ device and carried out a preliminary diagnostic. Lee[9] further investigated the CTLR-type plasma jet device at three microwave frequencies for plasma discharge morphology and electrical properties. Hrycak et al.[10] designed a coaxial transmission line (CTL)-type plasma jet device. The coaxial inner conductor of the device is divided into two segments with different radii, and the segment near the coaxial connector is thicker so that the input impedance can be matched; while the segment near the end is thinner so that the electric field strength at the end is higher, which is favorable for discharging. Since this plasma source can generate low-temperature plasma suitable for biological treatment, the researchers applied it for sterilization. Schopp et al. [11] conducted a detailed study on the thermodynamic and other properties of this CTL-type plasma jet device at different frequencies. Fu et al.[12] designed a microwave plasma jet device with a dual coaxial structure. The device had two layers of CTLs nested together, and the researchers used this device to generate a 28-mm plasma jet with a maximum efficiency of 89.6% in the absence of a matching system. Goel et al.[13] optimized the spatial parameters of the coaxial plasma jet device under different operating conditions and explained the experimental results with the numerical simulation results.

As mentioned above, the structure of devices utilizing microwave excitation to generate atmospheric pressure plasma can be broadly categorized into three types, which are waveguide-type, microstrip line-type, and coaxial-type structures. Compared with the other two structures, the coaxial-type device is simpler, more compact, and portable. However, most of the current coaxial jet generators are of the CTL type, and few research studies have been conducted on the CTLR type. The CTLR-type structure shows high efficiency and low power consumption, which can reduce the gas temperature of the plasma jet. In addition, argon (Ar) or helium (He) discharges were used in the majority of these studies, and other gas discharges were hardly studied.

In this article, based on a CTLR-type structure, a novel atmospheric pressure microwave plasma jet generator was designed with 2.45 GHz as the working frequency. The electric field strength of the jet generator was simulated by the electromagnetic field module of COMSOL Multiphysics. The characteristic dimensions of the device were adjusted to optimize the distribution of the electric field. After building the experimental apparatus based on the simulation, basic discharge morphology and multigas discharge experiments were implemented. After that, the electron excitation temperature (T_{exc}) and gas temperature (T_{g}) of the plasma jet were diagnosed by optical emission spectroscopy (OES). Finally, the surface treatment of polytetrafluoroethylene (PTFE) materials using the APPJ was also explored as a demonstration of preliminary application.

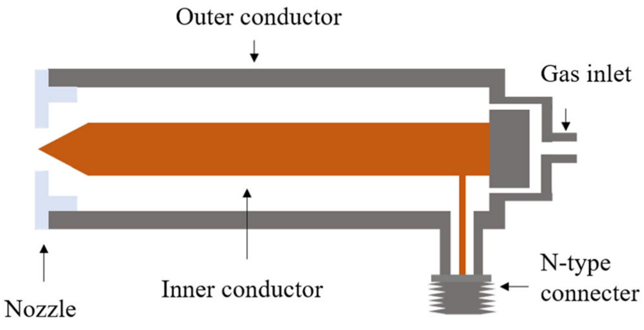

FIGURE 1 The schematic of the cross-section of the microwave atmospheric pressure plasma jet (MW-APPJ) generator.

2 | EXPERIMENTAL APPARATUS AND METHODS

2.1 | Description of plasma device

As mentioned above, coaxial plasma jet devices can be divided into two types: the CTL-type plasma jet generator and the CTLR-type plasma jet generator. The main structural difference between the two types of devices is the location of the microwave input ports. The CTL-type one has the feed direction coincide with the coaxial line and is connected directly through the coaxial connector, whereas the CTLR type has the feed port perpendicular to the coaxial line and is shorted at one end of the coaxial line.

In this article, a coaxial MW-APPJ device was designed based on the CTLR structure (see Figure 1). The main body of the generator was a CTL with an inner conductor (radius of 3 mm) and an outer conductor (inner radius of 7 mm). According to the coaxial line characteristic impedance calculation formula:

$$Z_0 \approx \frac{60}{\sqrt{\varepsilon_r}} \ln \frac{b}{a}. \tag{1}$$

Where Z_0 is the characteristic impedance, ε_r is the relative permittivity, and a and b denote the inner radius of the inner conductor and the inner radius of the outer conductor, respectively. Since the medium inside the coaxial device was air, here ε_r equaled to unity. Calculation results indicated that the characteristic impedance of the generator was 50.8 Ω. The coaxial length of the coaxial line resonator device was 30.5 mm, which approximately equaled to a quarter of the wavelength of 2.45 GHz microwave in the coaxial line. The device was a quarter-wavelength transmission line resonator, in which the electric field exhibited maximum strength at the open end. A polyetheretherketone (PEEK) nozzle was used at the outlet of the plasma generator for constraining the gas flow. In addition, the device herein was tapered at the end of the inner conductor so that the electric field at the tip was further enhanced for plasma generation.

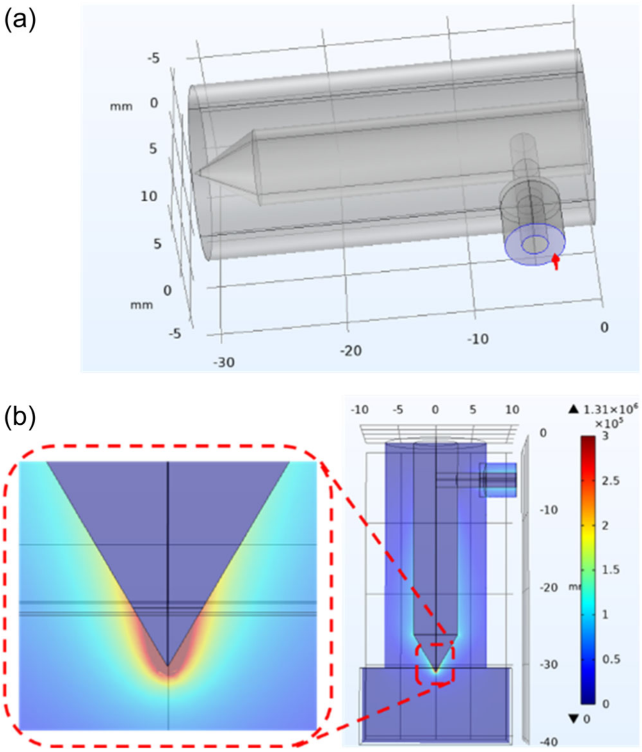

FIGURE 2 (a) The three-dimensional (3D) model and (b) the electric field distribution of the microwave atmospheric pressure plasma jet (MW-APPJ) generator.

2.2 | Simulation

The electric field distribution of the plasma jet generator was simulated and analyzed using the electromagnetic field module of COMSOL Multiphysics. In the COMSOL Multiphysics high-frequency electromagnetic field module, the following equation was used to calculate the electric field:

$$\nabla \times \mu_r^{-1}(\nabla \times E) - k_0^2\left(\varepsilon_r - \frac{j\sigma}{\omega\varepsilon_0}\right)E = 0. \tag{2}$$

A three-dimensional (3D) geometric model of the generator is shown in Figure 2a. All metal boundary parts in the model were replaced by surfaces without thickness, and ideal electrical conductor boundary conditions were used to simplify the model. The side power feed ports were set as coaxial feeds. The scattering boundary conditions were set at the open circuit end, and the interior space was partially filled with air.

As shown in Figure 2b, for the electric field distribution of the generator at an input power of 20 W, the highest electric field of the generator reached 1×10^6 V/m (see the enlarged part), exceeding the critical electric field of Ar discharge at atmospheric pressure (3×10^5 V/m). As can be seen from the electric field distribution in the simulation diagram, the tapering inner conductor tip effectively increased the local electric field, enabling the tip region to maintain plasma generation at low power, which constrained the gas temperature of the plasma. In addition, the use of a gradual structure rather than a sudden change prevented arc discharging caused by high field strengths between the inner and outer conductors.

2.3 | Apparatus

The experimental MW-APPJ system is shown in Figure 3, including a 2.45 GHz solid-state microwave source (Chengdu Wattsine Electronic Technology, WSPS-2450-200m), a coaxial three-stub tuner, a mass flow controller (Sevenstar Electronic Technology, D07-12A/ZM), and a self-designed plasma generator. The solid-state microwave source generated 1–200 W of microwaves at 2.45 GHz powered by a 27 V DC power supply (Mean Well Enterprise, RSP-750-27), and the power of the solid-state microwave source was controlled and displayed using a self-designed control module based on STM32 development board. This model of solid-state microwave source was equipped with an integrated circulator and a load; so, the forward input power and reflected power can be observed directly through the control module. The microwave was fed into the plasma generator via the coaxial three-stub tuner and the CTL. The Ar flow rate was controlled by the mass flow meter with a maximum of 10 standard liter per minute (SLM). The optical emission spectra (OES) of the Ar plasma jet were collected using a four-channel USB-type fiber optic spectrometer (Avantes, AvaSpec-2048TEC). The fiber optic probe was placed 3 mm from the jet nozzle and aimed at the bottom of the jet to collect the highest emission intensity. The spectral integration time was set as 1.05 ms for all measurements. The jet profiles were recorded using a digital camera with a complementary metal-oxide-semiconductor model of IMX803. The ISO was set to 200 and 50 when shooting Figures 7 and 8, respectively. The shutter speed was set to 1/2000 and 1/50 s when shooting Figures 7 and 8, respectively.

2.4 | Diagnostics of the MW-APPJ

The plasma can be considered near local thermodynamic equilibrium (LTE) in an atmospheric pressure microwave plasma flowing at a relatively low velocity (<120 m/s) because the convection rates are lower than the chemical reaction rates in this case.[14] Therefore, OES was used to determine the gas temperature and electron excitation temperature of the MW-APPJ.

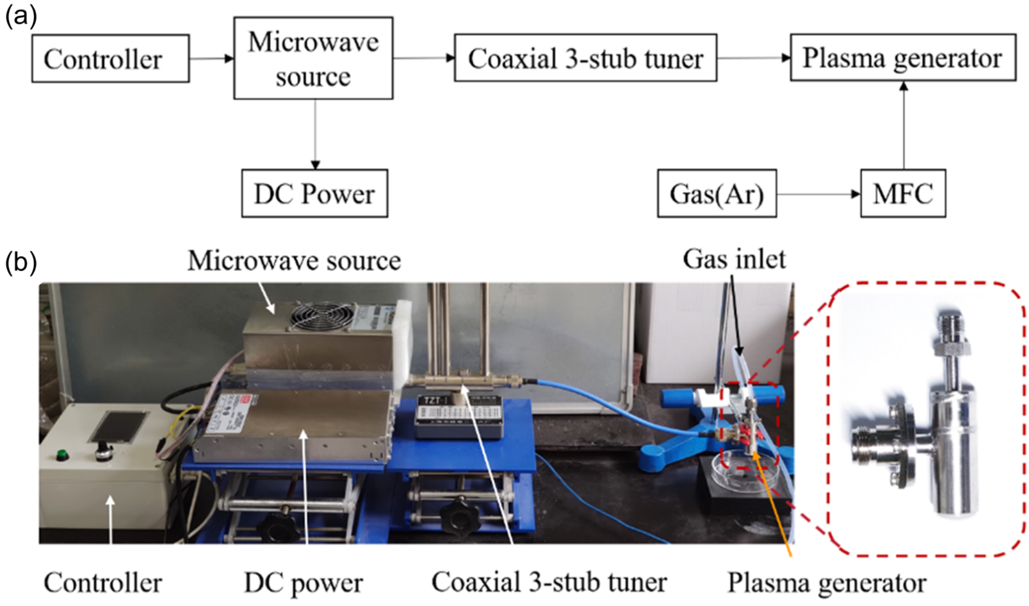

FIGURE 3 (a) Schematic of the experimental arrangement. (b) The apparatus of the microwave atmospheric pressure plasma jet (MW-APPJ) equipment.

TABLE 1 Ar atomic spectral lines and individual parameters.[16]

λ (nm)	A_{ki} (10^6 s^{-1})	g_k	E_k (eV)	Ref.
675.2834	1.93	5	14.7425	[17]
687.1289	2.78	3	14.7109	[17]
696.543	6.4	3	13.33	[17, 18]
706.7218	3.8	5	13.3022	[17, 18]
714.7042	0.63	3	13.2826	[17, 18]
727.2936	1.83	3	13.3279	[17, 18]
737.2118	1.9	9	14.7571	[17]
738.398	8.5	5	13.3022	[17, 18]
750.3869	45.0	1	13.4799	[17, 18]
751.4652	40.0	1	13.2730	[17, 18]
763.5106	24.5	5	13.1718	[17, 18]
801.4786	9.3	5	13.0949	[17, 18]
810.3693	25.0	3	13.1531	[17, 18]
811.5311	33.0	7	13.0757	[17, 18]
912.2967	18.9	3	12.9070	[17, 18]

Abbreviation: Ar, argon.

2.4.1 | Electron excitation temperature fitting method

The electron excitation temperature can be calculated by the Boltzmann plot method,[15] where the Boltzmann slope can be derived from the following equation:

$$\ln\left(\frac{I\lambda}{g_k A_{ki}}\right) = -\frac{E_k}{kT_{exc}} + C. \tag{3}$$

where λ is the wavelength of the emission spectral line, I is the relative intensity of the spectral line, g_k is the statistical weight of each energy state, A_{ki} is the transition probability, E_k is the energy of the upper energy level, k is the Boltzmann constant, and T_{exc} is the electron excitation temperature in Kelvin units. Thus, by linear fitting $\ln\left(\frac{I\lambda}{g_k A_{ki}}\right)$ and E_k, the electron excitation temperature can be obtained by the slope of the fitting curve. To improve the accuracy, the relative intensities of multiple spectral lines of the Ar atomic spectrum were chosen, and the calculations of the relevant parameters are shown in Table 1, which can be found in the National Institute of Standards and Technology Atomic Spectra Database.[16] As shown in Figure 4, a linear curve was fitted to the spectral data obtained by the MW-APPJ generator at 2 W and 1 SLM of Ar. The slope of the fitting curve was calculated to be −2.298, that is, the electron excitation temperature can be derived as 0.435 eV.

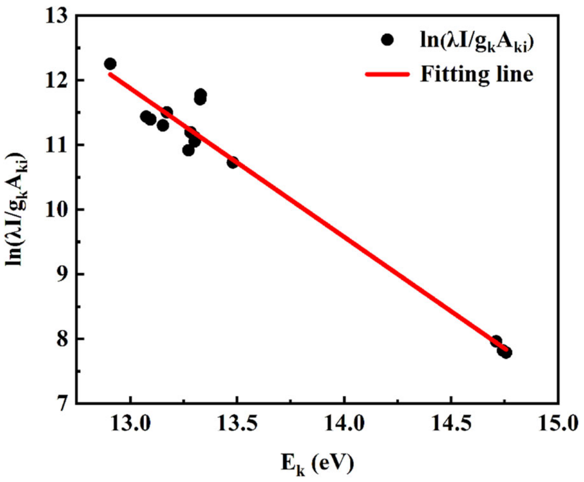

FIGURE 4 Sample Boltzmann plot for T_{exc} measurement at operating condition of 2 W and 1 standard liter per minute (SLM) of argon (Ar).

2.4.2 | Gas temperature fitting method

At near LTE, the gas temperature (T_g) approximately equals to the rotational temperature of the atmospheric pressure plasma due to its highly collisional nature and the almost complete exchange of rotational and translational kinetic energies between the heavy particles.[19] In the high-temperature environment of atmospheric pressure microwave plasma, H_2O molecules tend to ionize into OH radicals. Since the lifetimes of the ground-state OH radicals are usually much longer than the characteristic time between collisions and the OH radical spectra are easily distinguishable and hardly overlap with other spectral lines, the rotational temperature of the OH radicals provides a good representation of the plasma gas temperature.[20]

The OH-based spectra are mainly located in the 305–325 nm wavelength region, and the relative intensities of their spectral lines are determined by the rotational and vibrational temperatures. In particular, the region of 306–310 nm is mainly determined by the rotational temperature. Therefore, the gas temperature of atmospheric pressure microwave plasma was obtained by fitting the experimental spectra of the OH ($A^2\Sigma^+ \rightarrow X^2\Pi_r$) band in the 306–310 nm wavelength region to the theoretical spectra. The rotational temperature was adjusted at 10 K intervals by using the LIFBASE spectral simulation software. Figure 5 shows the fitted and experimental spectra of the MW-APPJ at 2 W and

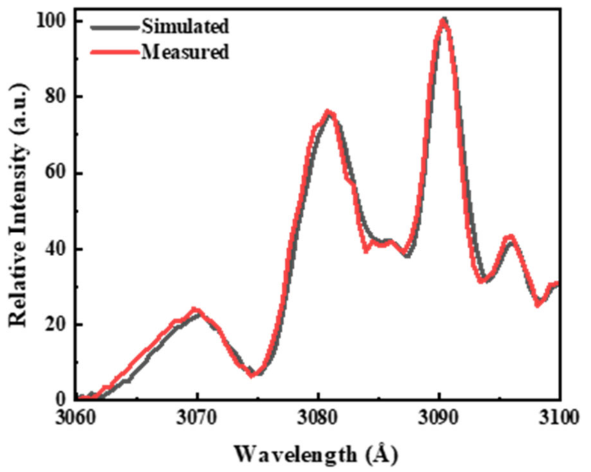

FIGURE 5 Measured optical emission spectroscopy (OES) spectrum and simulated spectrum from LIFBASE at operating conditions of 2 W and 7 standard liter per minute (SLM) of argon (Ar).

7 SLM of Ar. The rotational temperature was determined as 430 K, which equaled to the gas temperature. Due to the acquisition angle of the spectra, the gas temperature calculated from the fitting method is the upstream temperature of the jet. The downstream temperature of the jet was measured using a K-type thermocouple to visualize the tail end of the plasma gas temperature.

2.5 | PTFE material treatment

2.5.1 | Ar plasma treatment

PTFE was chosen as the model polymer because its wide applications in industries, such as automotive, chemical industry, electrical, and electronics. Commercially available square PTFE sheets of $10 \times 10 \times 1\,\text{mm}^3$ size were used as samples. They were cleaned with anhydrous ethanol before plasma treatment and dried at room temperature. The plasma experimental apparatus is shown in Figure 3. The surfaces of the samples were treated uniformly for 15–60 s using the MW-APPJ device at 10 W and 2 SLM of Ar.

2.5.2 | Characterization

The wettability of the samples was evaluated by water contact angle (WCA) measurements using an A-200 contact angle instrument (DropMeter) under static condition. The surface chemical composition and binding information were assessed by X-ray photoelectron spectroscopy (XPS) using a ThermoFisher Scientific Escalab 250Xi spectrometer equipped with an aluminum anode (Al $K_\alpha = 1486.6\,\text{eV}$). The surface morphology of the PTFE sheets was characterized by field emission scanning electron microscopy (FE-SEM), which was performed on a JSM-7500F microscope (JEOL (Beijing) Co., Ltd.) operated at 15 kV. Before SEM observations, the samples were coated by a gold sputtering coater for 5 min to prevent charging of the specimen.

2.6 | Preliminary experiment on anticipated applications

To demonstrate the potential applications of the MW-APPJ device, the feasibility of treating biological materials and agricultural products with the plasma jet was tested. The plasma jet was used to contact directly with the author's finger. The plasma jet was also used to treat a fresh cherry tomato that was bought from a local fruit store. For both experiments, the MW-APPJ device was operated at the condition of 5 W and 7 SLM of Ar.

3 | RESULT AND DISCUSSION

3.1 | Working window measurement and plasma morphology analysis

The stable operating window of the jet generator was first measured. The power range was determined to be 2 W–40 W. When the power was lower than 2 W, the electric field strength was not enough to maintain the gas discharge; so, the plasma only existed inside the nozzle or quenched; when the power was greater than 40 W, the jet was not stable and tended to convert to arc. The flow rate range was also determined. As the power increased, a larger Ar flow rate was required to maintain a stable plasma jet but below 10 SLM.

After the determination of the operating window, experiments were performed to investigate the change of jet length in stable working conditions. When studying the influence of flow rate on jet length, the power was fixed at 10 W. When studying the impact of power on jet length, the flow rate was fixed at 1 SLM. The dependence of jet length on gas flow rate and power is shown in Figure 6. As shown in Figure 6a, the jet length gradually reached maximum when the flow rate increased from 0.5 SLM to 1 SLM. Figure 6b demonstrates that the jet length increased from 1 to 10 mm as power increased from 1 to 5 W and remained in plateau with further power increment. In summary, the CTLR-type generator was capable of producing APPJ with a maximum length of 10 mm at low power and flow rate. The morphologies of MW-APPJ at different power when the Ar flow rate was fixed at 2 SLM are shown in Figure 7. The turbulence phenomenon at high flow rates was also investigated. In fluid mechanics, the Reynolds number that helps to predict the transition from laminar to turbulent flow is defined as $Re = v\rho d/\mu$, where v, ρ, d, and μ represent flow speed, fluid density, characteristic length (tube diameter), and dynamic viscosity, respectively. To reach a turbulence state, the Reynolds number should be greater than 2900,[21] and this derives a flow rate larger than ca. 5 SLM for the case of our jet device. We have recorded the jet profiles at different flow rates of 0.5, 1, and 5 SLM, as shown in Supporting Information S1: Figure S1. It can be seen from Supporting Information S1: Figure S1 that the plasma jet remained in a laminar flow state when the flow rate was 0.5 SLM. When the flow rate was 1 SLM, a tiny branch of plasma plume appeared, which may imply that the plasma jet was in the transition state. When the flow rate was further increased to 5 SLM, the jet profile became irregular, indicating that the plasma jet was in a turbulent flow state. A comparison of jet length, power, and flow rate of the MW-APPJ device in this work with those of reported ones in the literature is shown in Supporting Information S1: Table S1. It can be concluded from Supporting Information S1: Table S1 that the our CTLR-type MW-APPJ device possesses the advantage of producing plasma jet with acceptable length at low power and low flow rate, which may guarantee its application in a heat-sensitive scenario.

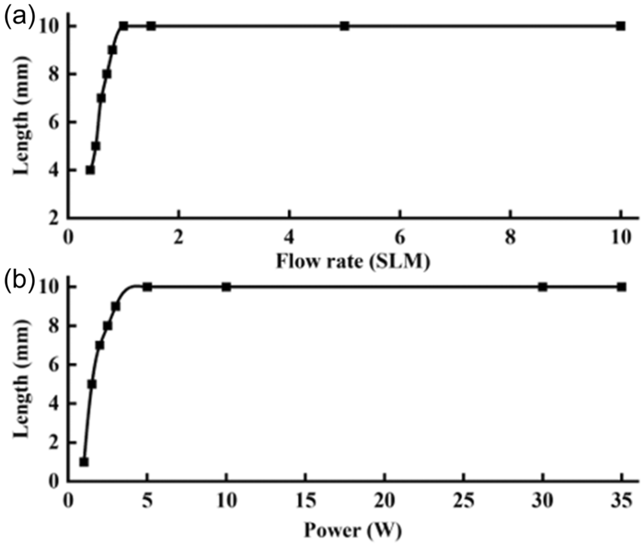

FIGURE 6 The dependence of jet length on (a) gas flow rate and (b) power.

In addition to pure Ar, the morphologies of MW-APPJ of Ar + O_2, Ar + N_2, Ar + NH_3, Ar + CO_2, pure N_2, and pure He were investigated, and the corresponding photos are shown in Figure 8. As can be seen in Figure 8, the jet lengths of these gases were shorter than those of pure Ar. This is because the molecular weight of Ar is heavier than that of reactive gases and He. So, Ar atoms can travel a longer distance after being ejected out of the nozzle. On the other hand, the lighter gases dilute much faster, which contributes to shorter jet lengths.

3.2 | Active species

For practical applications, besides jet length, the active species in the plasma jet is another important factor. The OES spectrum of Ar plasma jet at 1 SLM and 2 W is shown in Figure 9. Because the working gas is high-purity Ar (99.999%), the most obvious Ar I spectral lines can be seen in the spectrum. By zooming in on the range of 200–450 nm, distinct NH (A–X), OH (A–X), and NO (A–X) electronic bands can be distinguished, and a weak N_2 (C–B) second positive band can be seen overlapping with the NH(A–B) band. In addition, weak O (777 nm) spectral lines can also be observed. The chemical reactions

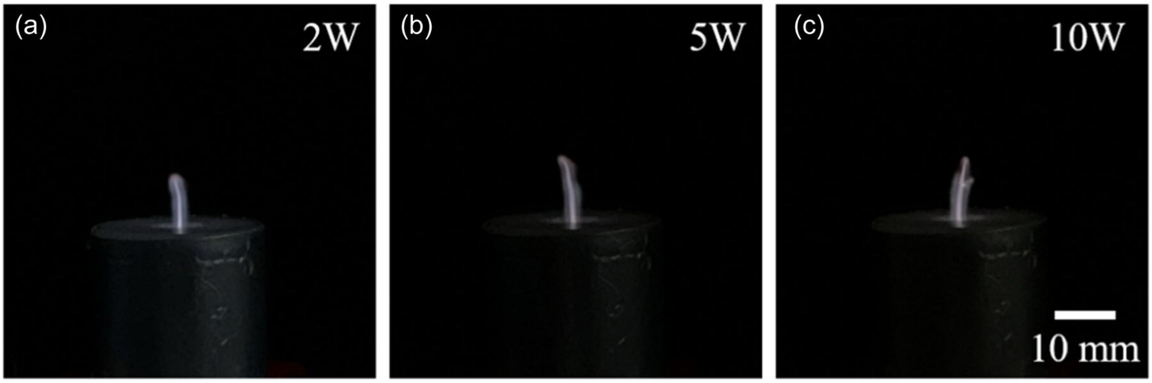

FIGURE 7 Argon (Ar) plasma jet profiles at operating conditions of (a) 2 W, (b) 5 W, (c) 10 W, and fixed flow rate of 2 standard liter per minute (SLM).

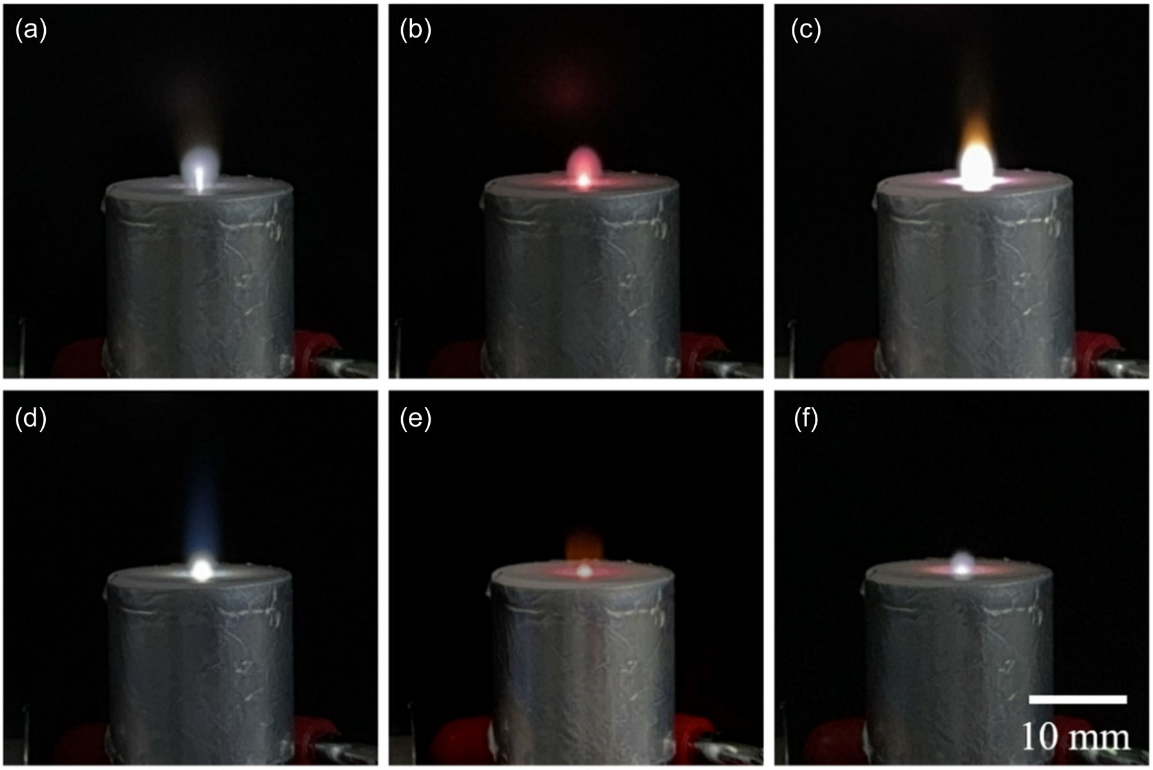

FIGURE 8 The morphologies of the microwave atmospheric pressure plasma jet (MW-APPJ) for different gases at a total flow rate of 2 standard liter per minute (SLM) and power of 40 W: (a) Ar + O_2 ($Ar/O_2 = 10:1$), (b) Ar + N_2 ($Ar/N_2 = 10:1$), (c) Ar + NH_3 ($Ar/NH_3 = 20:1$), (d) Ar + CO_2 ($Ar/CO_2 = 10:1$), (e) N_2, (f) He.

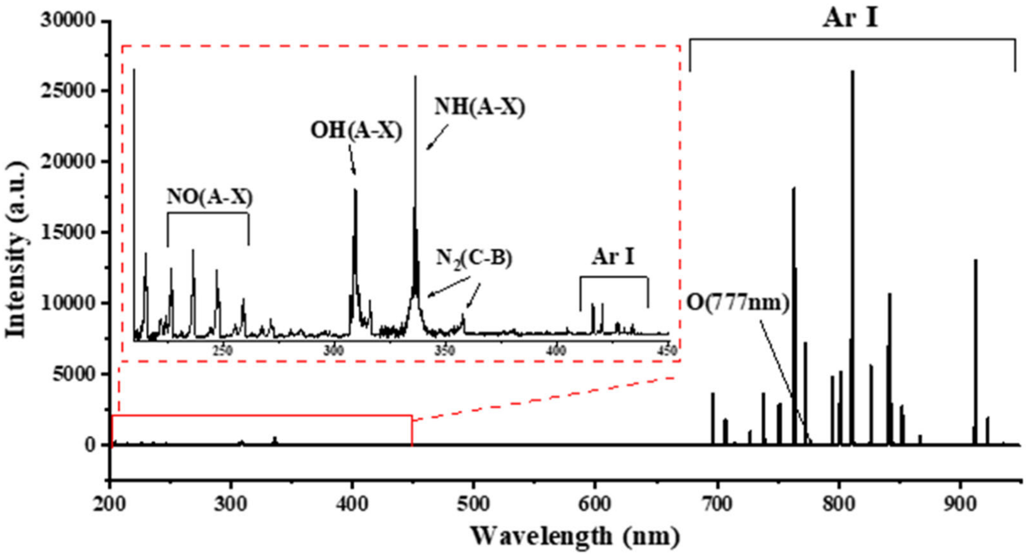

FIGURE 9 The optical emission spectroscopy (OES) spectrum of argon (Ar) plasma jet at operating condition of 1 standard liter per minute (SLM) and 2 W.

in plasma are very complex, often amounting to hundreds,[22] and the equations for the main reactions in the plasma jet are listed in Table 2. According to the OES spectrum, the main reactive species in the atmospheric pressure Ar plasma jet are Ar*, O, OH, NH, NO, and N_2*.

The spectral emission intensities of active species depend on the power and flow rate, which will be discussed below. Generally, as the power increases, the emission intensities of various active species increase since more energies are gained by the gaseous particles.[23] On the

TABLE 2 Main reactions of Ar plasma jet.

Reactions	No.
$e + H_2O \rightarrow H + OH + e$	R1
$e + Ar \rightarrow Ar^* + e$	R2
$e + N_2 \rightarrow N_2^* + e$	R3
$e + O_2 \rightarrow 2O + e$	R4
$N + OH \rightarrow NO + H$	R5
$N + H_2O \rightarrow OH + NH$	R6

Abbreviation: Ar, Argon.

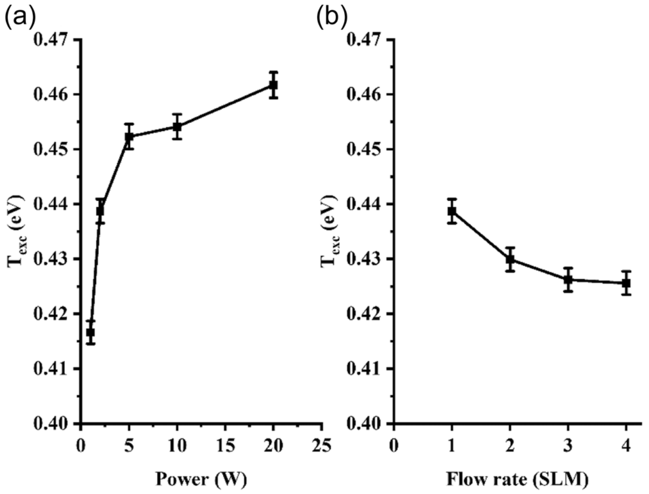

FIGURE 10 The variation of T_{exc} with (a) input power and (b) gas flow rate.

other hand, the emission intensities of active species (such as OH and NH) usually first increase and then decrease with the increasing flow rates of reactive gases.[24] This is because, when the reactive gases are introduced, the collision between energetic electrons and gas molecules produces more active species, thus enhancing the emission intensity. However, since the reactive gases are electronegative, further increasing the flow rate results in the energetic electrons being captured by the gas molecules. As a result, the collision and ionization processes that are responsible for active species production are weakened, and their spectral emission intensities decrease.

3.3 | Electron excitation temperature (T_{exc})

The electron excitation temperature of the MW-APPJ was calculated as a function of power and Ar flow rate by the Boltzmann plot method mentioned above (see Figure 4). At a fixed Ar flow rate of 1 SLM, the variation of T_{exc} with power is shown in Figure 10a, where T_{exc} first increased and then gradually leveled off as the power gradually increased. In the low power range, an increase in power significantly enhanced the energy of electrons, leading to a rapid increase in T_{exc}. In the high power range, the energy loss of electrons was prominent due to the high collision frequency, which resulted in a lower growth rate of T_{exc}. By increasing the microwave power from 1 to 20 W, T_{exc} was elevated from 0.42 to 0.46 eV. As shown in Figure 10b, at a fixed power of 2 W, T_{exc} first decreased rapidly with higher gas flow rates and then stabilized. The decrement of T_{exc} with increasing Ar flow rate from 1 SLM to 4 SLM was about 0.015 eV, which suggests that gas flow rate has a relatively limited effect on the electron excitation temperature compared with power.

3.4 | Gas temperature (T_g)

The gas temperature of APPJ is a key parameter, and plasma jets with sufficiently low temperatures do not cause thermal damage to materials and are therefore better able to be used in medical and material processing applications. The gas temperatures of the jet centers ($T_{g,c}$) obtained by fitting using LIFBASE software are shown in Figure 11. At a fixed flow rate, $T_{g,c}$ increased from 580 to 680 K as input power was elevated from 1 to 20 W. At a fixed input power, $T_{g,c}$ decreased from 630 K to 460 K as gas flow rate increased from 1 SLM to 5 SLM. The gas temperatures at downstream of the jets ($T_{g,d}$) were measured by the K-type thermocouples and are shown in Figure 11. $T_{g,d}$ had the same trend as $T_{g,c}$, but the values of $T_{g,d}$ were lower than those of $T_{g,c}$ by ~250 K. The minimum value of $T_{g,d}$ was only 320 K, which implied potential applications in low-temperature materials processing scenario.

3.5 | Characterizations of PTFE modified by MW-APPJ

The MW-APPJ device has the advantages of low temperature, easy handling, and high portability. To demonstrate the potential of practical applications of the MW-APPJ device, hydrophilicity improvement of PTFE materials was used as an example. The changes of material properties after plasma jet treatment were characterized by wettability, morphology, and composition measurement.

3.5.1 | Water contact angle (WCA) measurements

Figure 12 shows the variation of WCA with plasma treatment duration of PTFE samples treated by Ar

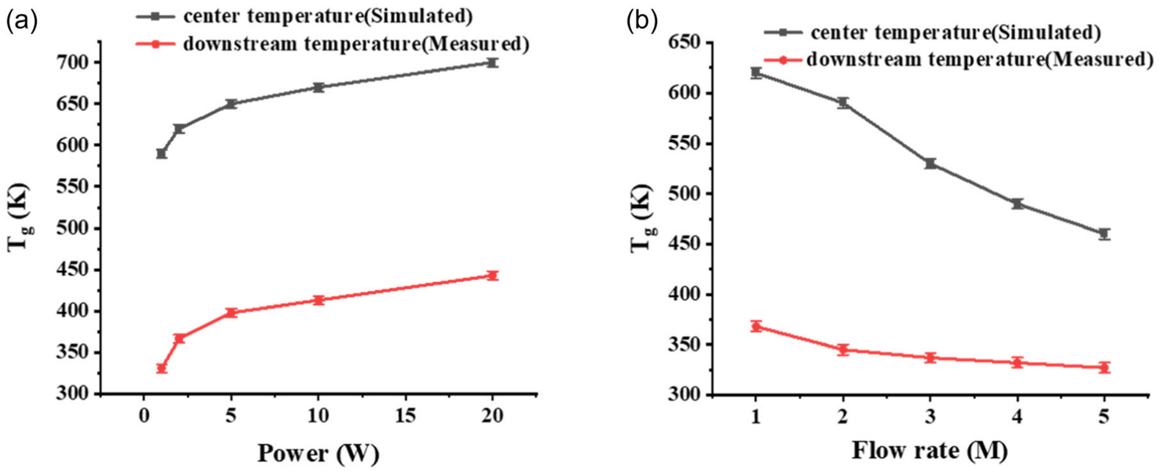

FIGURE 11 Variation of plasma jet gas temperature with (a) input power and (b) gas flow rate.

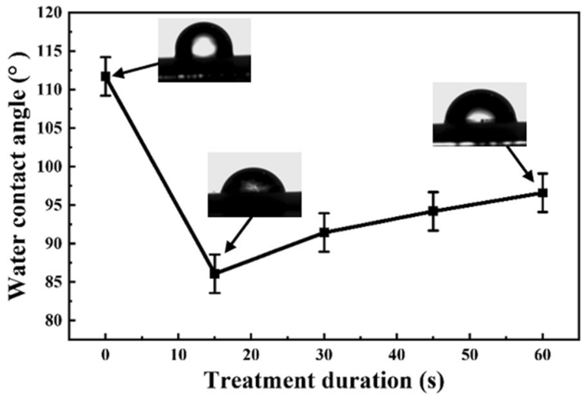

FIGURE 12 The variation of polytetrafluoroethylene (PTFE) water contact angle with plasma jet treatment duration and photographs at selected durations.

plasma jet. The WCA of the pristine sample was 111.7 °, which decreased to approximately 86.1° after 15 s of plasma jet treatment. Since the plasma jet device was placed in an open environment, the discharge contained a variety of oxygen-containing species (as mentioned in the OES diagnostics), and thus, hydrophilic groups were introduced onto the surface of the PTFE sheets by plasma treatment. A comparison table of hydrophilicity improvement in this work with other reported results in the literature is exhibited in Supporting Information S1: Table S2 to show the benefits of the designed microwave jet source on surface treatment. It can be seen that, thanks to the high density of active species produced by the microwave plasma jet, the hydrophilicity improvement effect of PTFE treated by MW-APPJ was more significant than that of PTFE treated by other types of plasma jets. However, when the PTFE sample was treated for more than 15 s, the WCA started to increase and reached 96.6° after 60 s of treatment. This is because prolonged plasma treatment induced an etching process on the PTFE surface, which led to an increase in surface roughness and also destroyed some of the hydrophilic groups, resulting in higher WCA values.[25,26] Since both the chemical composition and morphology of the materials surface affect the wettability, both features were studied and discussed below.

3.5.2 | XPS results

XPS measurements were conducted to evaluate the chemical composition of the PTFE samples before and after plasma treatment. XPS survey scans were acquired to determine the percentages of elements, and the results are shown in Table 3. It can be seen that after 15 s of Ar plasma treatment, the F/C atomic ratio significantly reduced, and the O/C ratio slightly increased, indicating that the fluorine atoms on the polymer chains were removed while oxygen-containing hydrophilic groups were grafted. After prolonged plasma treatment, the F/C ratio bounced almost back to the untreated level, and oxygen content retained in a relatively low level.

To further understand the change of chemical bonding on the surface of plasma-treated PTFE sheets, the high-resolution C 1s spectra of pristine and Ar plasma-treated PTFE sheets were analyzed. As shown in Figure 13, the C 1s spectrum of pristine PTFE was deconvoluted into two contributions: the major peak with a binding energy of 292.2 eV corresponded to the C–F_2, and the smaller peak with a binding energy of 284.8 eV corresponded to C–C/C–H. After 15 s of plasma treatment, the intensity of C–F_2 groups decreased, while the intensity of C–C/C–H bonds enhanced dramatically. Besides, a small peak of C═O groups (288.6 eV) appeared at this treatment duration.[27] When the treatment duration was prolonged to 30 s or longer, the peak of C–F_2 groups rebounded, and the C═O groups were converted to O–C═O groups (289.3 eV). These results clearly demonstrate that after a short duration of plasma treatment, fluorine atoms were removed from the PTFE surface, and oxygen-containing hydrophilic groups were grafted onto the PTFE surface.

TABLE 3 The atomic composition of untreated and plasma-treated PTFE samples.

Treatment duration(s)	F (%)	C (%)	O (%)	F/C	O/C
0	67.62	31.80	0.58	2.13	0.02
15	35.59	58.29	6.12	0.61	0.10
30	66.48	32.08	1.43	2.07	0.04
60	66.68	31.93	1.40	2.08	0.04

Abbreviation: PTFE, polytetrafluoroethylene.

Figure 14a shows the O 1 s spectra of PTFE before and after Ar plasma treatment. The peak in the spectrum of untreated samples was weak and can be considered from contamination. After plasma treatment, the peak intensity of C–O/C═O (at 532.2 eV) [28] first increased and then decreased. The trend of peak intensity of C–O/C═O was similar to that of C–C/C–H. On the other hand, as shown in Figure 14b, the intensity of F1s peak at 689 eV decreased significantly after 15 s of plasma treatment and rebounded back to almost the same intensity level after prolonged treatment.

It can be deduced from the XPS results that the C–C and C–F bonds were broken and grafted with oxygen-containing functional groups within short plasma treatment. As the treatment duration was prolonged, the content of oxygen-containing functional groups tended to saturate first.[29] However, with further prolonged plasma treatment, the etching effect began to be prominent, and thus, the oxygen-containing groups

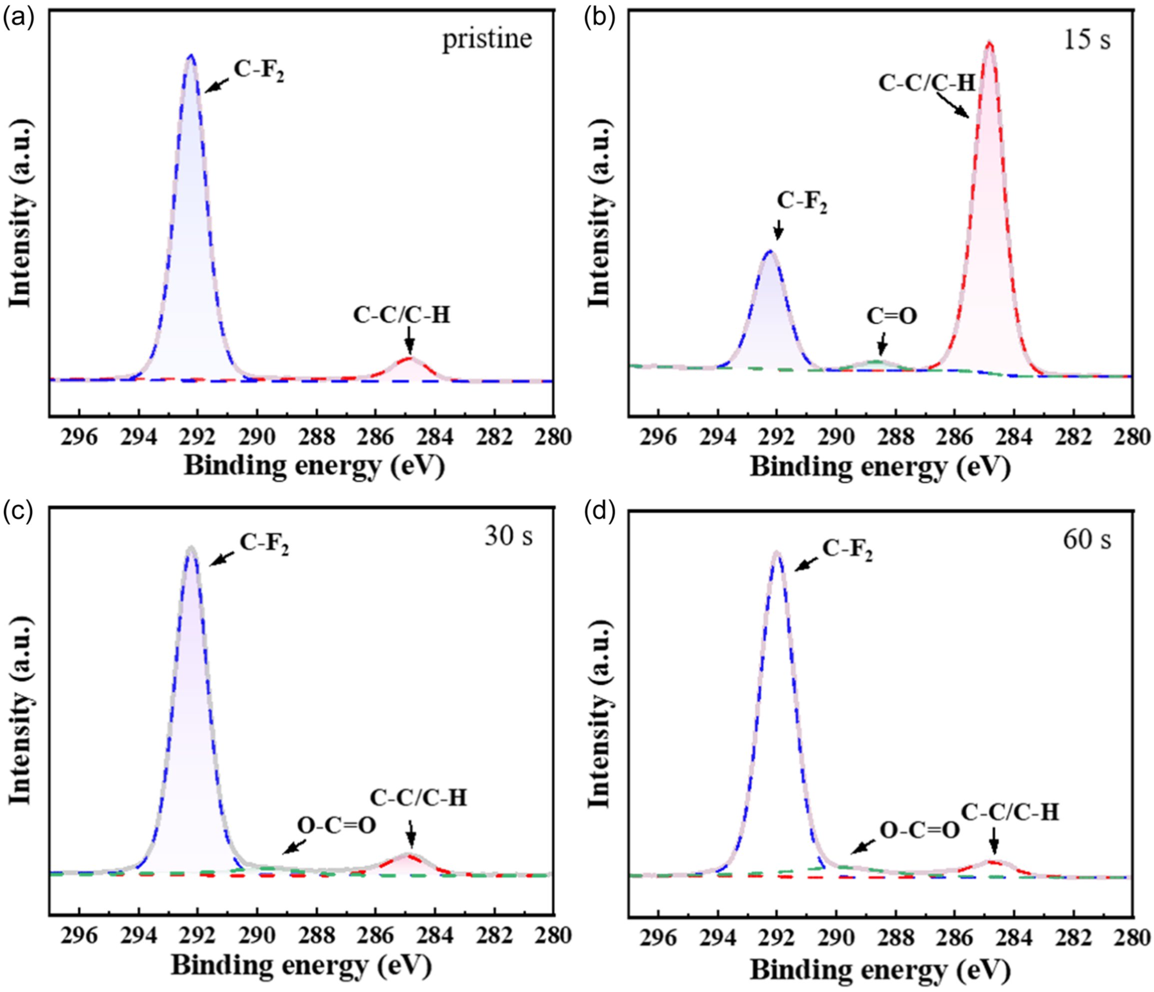

FIGURE 13 High-resolution C 1 s spectra of (a) pristine polytetrafluoroethylene (PTFE) and PTFE treated with argon (Ar) plasma for (b)15 s, (c) 30 s, and (d) 60 s.

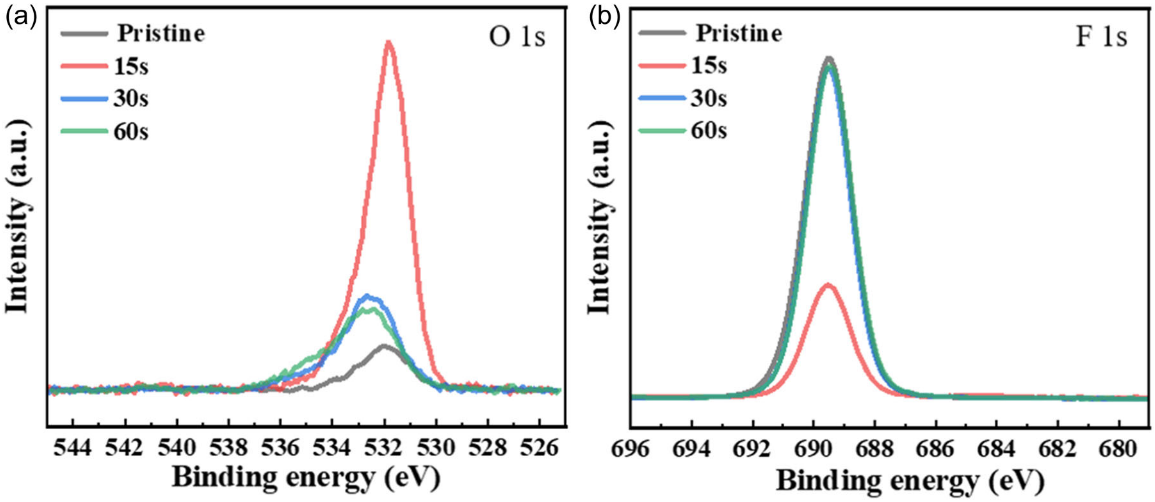

FIGURE 14 X-ray photoelectron spectroscopy (XPS) spectra of the polytetrafluoroethylene (PTFE) samples before and after plasma treatment. (a) O 1 s spectra and (b) F 1 s spectra.

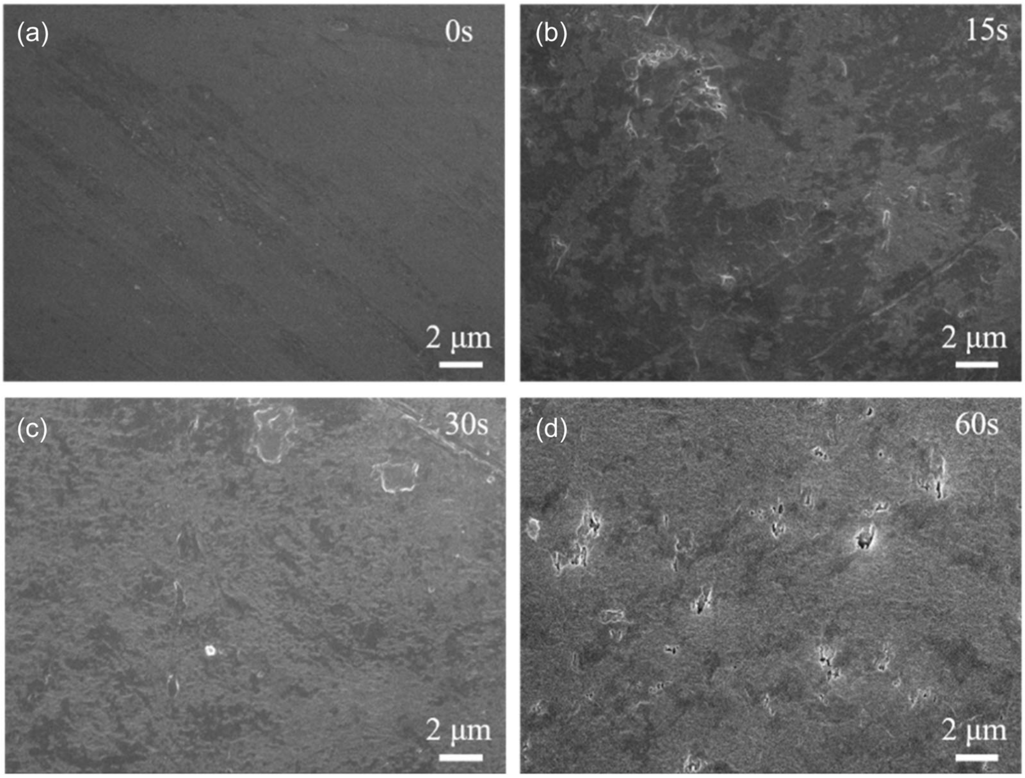

FIGURE 15 Field emission scanning electron microscopy (FE-SEM) images of (a) pristine polytetrafluoroethylene (PTFE) and PTFE treated with (b)15 s, (c) 30 s, (d) 60 s of argon (Ar) plasma treatment.

were partially destroyed, and subsurface fluorine atoms were exposed. It has been reported that the grafted oxygen-containing functional groups help to enhance the hydrophilicity while the fluorine atoms are strongly hydrophobic.[30] The XPS results explained the reason for Ar plasma treatment changing the hydrophilicity of the PTFE surface.

3.5.3 | Surface morphology characterizations: The morphology of pristine PTFE sample was investigated by FE-SEM

As shown in Figure 15a, it was found that the surface morphology of the pristine PTFE sheet was smooth. Figure 15b–d shows the FE-SEM images of PTFE samples after Ar plasma treatment for 15, 30, and 60 s, respectively. It can be seen from Figure 15b that the surface of the PTFE was still relatively smooth after a short-time plasma treatment, but some evidence of plasma etching appeared. Figure 15c,d shows that longer plasma treatment duration (30 or 60 s) induced severe etching, which dramatically changed the morphology of PTFE surface. After 30 s of plasma treatment, some mounds appeared as residual degradation products, and even cracks and holes appeared after 60 s of plasma treatment. With prolonged plasma treatment duration, the number of pits and humps increased, which indicated increasing surface roughness that contributed to reducing the surface hydrophilicity.

Combining the above characterization results, the mechanism of plasma modifying PTFE surface can be revealed. According to the OES diagnostic results, a variety of oxygen-containing species existed in the MW-APPJ, as the Ar plasma jet was generated in open space. For short plasma treatment duration (less than 15 s), the bombardment effect of Ar* in plasma mainly removed the fluorine atoms and broke the C–C bonds. This explains the reason why the F 1 s peak of the sample with 15 s of plasma treatment exhibited lowest intensity. Meanwhile, the oxygen species in plasma were grafted onto the dangling bonds of carbon atoms, explaining the highest intensity of the O 1 s peak in the sample treated with 15 s of plasma. The grafting of oxygen-containing groups accounts for the improvement in hydrophilicity. After 15 s of plasma treatment, the hydrophilicity of PTFE surface increased because of oxygen-containing groups grafting. For longer plasma treatment duration (more than 15 s) since more C–C bonds in the surface layer were destroyed, carbon atoms and oxygen functional groups were etched away. As a result, the O 1 s peak intensities of these samples dramatically decreased. On the other hand, because the surface layer was etched and the fluorine atoms in subsurface layer were exposed, the F 1 s peaks of these samples exhibited almost identical intensities as the pristine sample. The exposure of sublayer fluorine atoms also contributed to the decrease in hydrophilicity. A schematic picture of Ar APPJ modifying PTFE is shown in Supporting Information S1: Figure S2. It can be concluded that the hydrophilicity of a polymer surface can be modified using the MW-APPJ device developed in this work because the mechanisms mentioned above should be applicable to other polymer materials.

3.6 | A map of anticipated applications of the MW-APPJ device

To demonstrate the feasibility of treating biological materials with the MW-APPJ device, the compatibility of the plasma jet with human skin was tested. As shown in Supporting Information S1: Figure S3, the Ar plasma jet can be touched by human skin, and no overheating effect occurred. This implies the plasma jet can be used to directly treat a biological surface including human skin and dental gums. Since it has been reported in the literature that the reactive oxygen-nitrogen species possess a high capability of sterilizing,[31] it can be envisaged that the MW-APPJ device can be used in the sterilization of perishable agricultural products. The Ar plasma jet was used to treat the surface a cherry tomato. As exhibited in Supporting Information S1: Figure S3, after 30 s of plasma treatment, the surface of the cherry tomato remained intact, demonstrating that the plasma treatment will not destroy the vegetables' surfaces. This implies that the MW-APPJ device possesses the application potential of agricultural product sterilization. Further research on the applications of the MW-APPJ device in treating biological materials and agricultural products will be conducted in the future.

4 | CONCLUSION

This article reports an MW-APPJ generator based on a CTL resonator structure with a novel inner conductor geometry. The device was capable of generating an electric field of ~10^6 V/m at 2.45 GHz, as revealed by numerical simulations. A ~ 10 mm-length Ar plasma jet by self-igniting was obtained at an input power of ~20 W and maintained at a minimum power of 2 W. In addition to pure Ar discharges, discharge studies of multi-gas and multi-operating conditions were conducted. OES diagnostics determined the active species that the Ar plasma jet contained. The electron excitation temperature and gas temperature of the Ar plasma jet were diagnosed. The MW-APPJ device was used for surface modification of PTFE sheets. The surface hydrophilicity of PTFE sheets was improved after plasma jet treatment for a reasonable duration, validating the potential of the MW-APPJ device in surface modifications of polymer materials. The mechanism of changing surface hydrophilicity of PTFE materials by plasma jet treatment was revealed based on compositional and morphological characterization results.

ACKNOWLEDGMENTS

This work was financially supported by the National Natural Science Foundation of China (Nos. 12175035, 12375251, and 12005128), Open fund of State Key Laboratory of Advanced Electromagnetic Technology (No. 2022KF009), and the Fundamental Research Funds for the Central Universities (No. 2232024D-29).

CONFLICT OF INTEREST STATEMENT

The authors declare no conflict of interest.

DATA AVAILABILITY STATEMENT

The data that support the findings of this study are available from the corresponding author upon reasonable request.

ORCID

Dai Zhang http://orcid.org/0000-0003-1088-4201
Zilan Xiong http://orcid.org/0000-0003-1095-3959

REFERENCES

[1] J. Mizeraczyk, M. Dors, M. Jasiński, B. Hrycak, D. Czylkowski, *Eur. Phys. J. Appl. Phys*. **2013**, *61*, 24309.
[2] D. Li, M. Xiong, S. Wang, X. Chen, S. Wang, Q. Zeng, *Appl. Surf. Sci*. **2020**, *503*, 144257.
[3] I. N. Antonov, V. V. Komarov, A. V. Durakov, *IEEE Trans. Plasma Sci*. **2022**, *50*, 2845.
[4] L. Di, J. Zhang, X. Zhang, *Plasma. Process. Polym*. **2018**, *15*, 1700234.
[5] T. Takahashi, Y. Takao, K. Eriguchi, K. Ono, *J. Phys. D: Appl. Phys*. **2008**, *41*, 194005.
[6] M. Laroussi, T. Akan, *Plasma Processes Polym*. **2007**, *4*, 777.
[7] Z. Q. Chen, D. Hu, M. H. Liu, G. Q. Xia, X. L. Zheng, Y. L. Hu, Q. B. Ye, M. G. Chen, L. J. Zhu, X. W. Hu, *Chin. Phys. B* **2014**, *23*, 035202.
[8] J. Choi, F. Iza, H. J. Do, J. K. Lee, M. H. Cho, *Plasma Sources Sci. Technol*. **2009**, *18*, 025029.
[9] H. W. Lee, S. K. Kang, I. H. Won, H. Y. Kim, H. C. Kwon, J. Y. Sim, J. K. Lee, *Phys. Plasmas* **2013**, *20*, 123506.
[10] B. Hrycak, M. Jasiński, J. Mizeraczyk, *Eur. Phys. J. D* **2010**, *60*, 609.
[11] C. Schopp, H. Heuermann, M. Marso, *IEEE Trans. Plasma Sci*. **2017**, *45*, 932.
[12] W. Fu, C. Zhang, C. Nie, X. Li, Y. Yan, *Appl. Phys. Lett*. **2019**, *114*, 254106.
[13] V. Goel, R. Kar, A. Roy, D. S. Patil, N. Maiti, *IEEE Trans. Plasma Sci*. **2022**, *50*, 3539.
[14] C. O. Laux, T. G. Spence, C. H. Kruger, R. N. Zare, *Plasma Sources Sci. Technol*. **2003**, *12*, 125.
[15] B. Zhang, Q. Wang, G. Zhang, S. Liao, *J. Appl. Phys*. **2014**, *115*, 043302.
[16] A. Kramida, Y. Ralchenko, J. Reader, and NIST ASD Team**2023**, "NIST Atomic Spectra Database Lines Form", Version 5.11. https://doi.org/10.18434/T4W30F
[17] G. Norlén, *Phys. Scr*. **1973**, *8*, 249.
[18] W. L. Wiese, J. W. Brault, K. Danzmann, V. Helbig, M. Kock, *Phys. Rev. A*. **1989**, *39*, 2461.
[19] P. Bruggeman, F. Iza, P. Guns, D. Lauwers, M. G. Kong, Y. A. Gonzalvo, C. Leys, D. C. Schram, *Plasma Sources Sci. Technol*. **2010**, *19*, 015016.
[20] P. J. Bruggeman, N. Sadeghi, D. C. Schram, V. Linss, *Plasma Sources Sci. Technol*. **2014**, *23*, 023001.
[21] K. V. Sharp, R. J. Adrian, *Exp. Fluids* **2004**, *36*, 741.
[22] C. Wang, N. Srivastava, *Eur. Phys. J. D* **2010**, *60*, 465.
[23] Y. Liu, Z. Fang, J. Yang, *High Power Laser Part. Beams* **2013**, *25*, 2592.
[24] S. Yi, F. Liu, Z. Fang, *High Volt. Eng* **2019**, *45*, 1936.
[25] A. Sarani, N. De Geyter, A. Y. Nikiforov, R. Morent, C. Leys, J. Hubert, F. Reniers, *Surf. Coat. Technol*. **2012**, *206*, 2226.
[26] L. Lin, L. Rui, C. Li, Q. Liu, S. Li, Y. Xia, H. Hu, W. Yang, H. Xu, *J. CO2 Util*. **2021**, *53*, 101752.
[27] S. W. Fitriani, S. Ikeda, M. Tani, H. Yajima, H. Furuta, A. Hatta, *Mater. Chem. Phys*. **2022**, *282*, 125974.
[28] W. H. Lee, J. G. Lee, P. J. Reucroft, *Appl. Surf. Sci*. **2001**, *171*, 136.
[29] D. Lojen, R. Zaplotnik, G. Primc, M. Mozetič, A. Vesel, *Appl. Surf. Sci*. **2022**, *598*, 153817.
[30] F. Chen, W. Xu, Y. Lu, J. Song, S. Huang, L. Wang, I. P. Parkin, X. Liu, *Micro & Nano Lett* **2015**, *10*, 105.
[31] J.-H. Cheng, X. Lv, Y. Pan, D.-W. Sun, *Trends Food Sci. Technol*. **2020**, *103*, 239.

SUPPORTING INFORMATION

Additional supporting information can be found online in the Supporting Information section at the end of this article.

How to cite this article: D. Zhang, S. Xu, Z. Hou, X. Chang, Z. Wu, Z. Xiong, *Plasma. Process. Polym*. **2024**, e2400078. https://doi.org/10.1002/ppap.202400078